The Role of Organ of Corti Mass in Passive Cochlear Tuning

Ombeline de La Rochefoucauld* and Elizabeth S. Olson†
*Department of Otolaryngology, Head and Neck Surgery, and †Department of Otolaryngology, Head and Neck Surgery and Biomedical Engineering, Columbia University, New York, New York

ABSTRACT The mechanism for passive cochlear tuning remains unsettled. Early models considered the organ of Corti complex (OCC) as a succession of spring-mass resonators. Later, traveling wave models showed that passive tuning could arise through the interaction of cochlear fluid mass and OCC stiffness without local resonators. However, including enough OCC mass to produce local resonance enhanced the tuning by slowing and thereby growing the traveling wave as it approached its resonant segment. To decide whether the OCC mass plays a role in tuning, the frequency variation of the wavenumber of the cochlear traveling wave was measured (in vivo, passive cochleae) and compared to theoretical predictions. The experimental wavenumber was found by taking the phase difference of basilar membrane motion between two longitudinally spaced locations and dividing by the distance between them. The theoretical wavenumber was a solution of the dispersion relation of a three-dimensional cochlear model with OCC mass and stiffness as the free parameters. The experimental data were only well fit by a model that included OCC mass. However, as the measurement position moved from a best-frequency place of 40 to 12 kHz, the role of mass was diminished. The notion of local resonance seems to only apply in the very high-frequency region of the cochlea.

INTRODUCTION

Introduction to experimental design

The plunging motion of the stapes launches a traveling wave down the cochlea that peaks at frequency-dependent locations: low frequencies travel deep into the cochlea and peak in the apex, high frequencies peak in the base. The physical basis for the wave is the interaction between the mass of the cochlear fluid and the stiffness of the organ of Corti complex (OCC, the cellular tissue of the organ of Corti and the basilar and tectorial membranes on either side). The stiffness of the OCC is determined by its width, thickness, elasticity, and degree of longitudinal coupling. From base to apex, there is a decrease of OCC stiffness. The wave speed and therefore the wavelength (λ) decreases with decreasing stiffness. The reduced speed leads to growth of the wave due to conservation of energy; eventually, however, damping causes the response to plummet (1). Thus, the wavelength of the traveling wave will become shorter as the wave approaches and then passes the best-frequency (BF) place where it peaks (Fig. 1 *A*). The frequency tuning arises through the interaction of the cochlear fluid mass, the stiffness of the OCC, fluid and/or tissue viscosity, and possibly OCC mass. The anatomical OCC mass can be translated to height ($m_{occ} = \rho h$) if we assume that its density is approximately that of water ($\rho =$ 1 g/cm^3). From base to apex, the gerbil OCC height varies from 125 μm to 200 μm (2), therefore we expect the OCC mass to be $\sim$0.015 g/cm^2. However, because of its soft, liquid character, the OCC might be mechanically indistinguishable from the surrounding fluid, in which case the anatomical height would have diminished mechanical significance. The role of OCC mass in passive tuning is uncertain, and by studying the traveling wave pattern, we examine this role. Because active tuning is built upon a substrate of passive tuning, our conclusions will be important to cochlear mechanics in general.

In three-dimensional (3D) cochlear computer models, tuning can arise through the interaction of cochlear fluid mass and OCC stiffness without local mass, supporting the concept of nonresonant tuning. In their model, Steele and Taber (3,4) treated the cochlear partition as a plate of viscoelastic material, clamped at the sides. They referred to its mass as ''BM mass'', the basilar membrane mass; they considered the soft cellular tissue of the organ of Corti to deform with fluid pressure as though the cells were mechanically equivalent to fluid. Therefore, only the BM mass was expected to behave mechanically as a solid body. They explicitly studied the effect of this BM mass on tuning, and found that it was of little influence unless its value was unrealistically large (50 times bigger than the mass due to BM height), and concluded that BM mass could and should be neglected. Siebert (5) in a two-dimensional model and Zwislocki (6) in a one-dimensional model similarly concluded that OCC mass could be excluded with no significant effect on the tuning. More recent models

Submitted March 29, 2007, and accepted for publication July 20, 2007.

Address reprint requests to O. de La Rochefoucauld, E-mail: or2107@columbia.edu.

Abbreviations used: λ, wavelength of the traveling wave (cm); m_{occ}, OCC effective mass/unit area (g/cm^2); ρ, fluid density (g/cm^3), S, OCC stiffness/unit area (dyne/cm^3); f_r, resonant frequency (Hz); k, local wavenumber of the traveling wave (1/cm); P_{ST}, scala tympani pressure close to the OCC (dyne/cm^2); P_{SV}, scala vestibuli pressure close to the OCC (dyne/cm^2); Z_{occ}, OCC specific acoustic impedance (dyne s/cm^3); $\omega = 2\pi f$, radial frequency (radian/s); R, *OCC* resistance/unit area (dyne s/cm^3); z, v_z, a_z, displacement, velocity, and acceleration of OCC perpendicular to its local plane (cm, cm/s, cm/s^2); $h_{eq} = Q$, equivalent height of the fluid (cm); m_{fluid}, effective fluid mass (g/cm^2); h, height of the scala (cm); b, scala width (cm); ε, BM width (cm); b_0, parameter for the model (unitless); k_{exp}, experimental wavenumber (1/mm); d, longitudinal distance along OCC (cm); and φ, phase (radians).

Editor: Kevin D. Costa.

0006-3495/07/11/3434/17 $2.00

doi: 10.1529/biophysj.107.109744

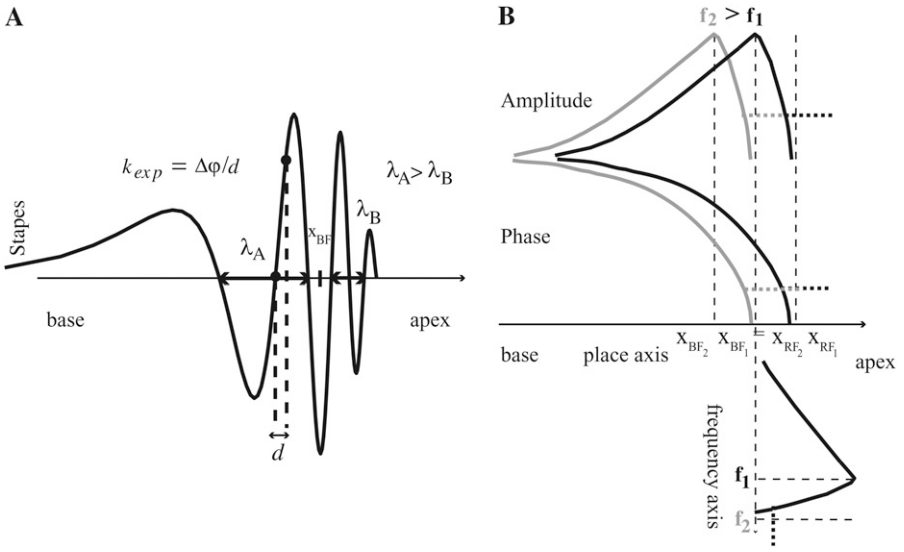

FIGURE 1 (*A*) Cartoon of a cochlear traveling wave illustrates the decrease of the wavelength as the wave reaches its best frequency place, X_{BF} (position of maximum amplitude response) and passes it. At each position the wave is characterized by an amplitude and phase. These are found by performing a FFT on the motion response to pure tone stimuli, over a range of frequencies, one position at a time. The phase difference ($\Delta\varphi$) between two closely spaced longitudinal positions, divided by the distance between them (d), gives the wavenumber (k_{exp}) at a position located in between the two points. The wavenumber is directly proportional to the inverse wavelength ($1/\lambda$). In practice, only a short longitudinal region is probed; in our case, that was an approximate millimeter length in the base of the ~11 mm gerbil cochlea (31). (*B*) Theoretical effect of local resonance. Illustrative amplitude and phase response curves for pure tone stimuli at two frequencies as a function of location are shown in the top curves. To illustrate the influence of local resonance, the solid curves are drawn based on a scenario in which the local resonant frequency is slightly greater than the best (peak) frequency. (In the alternative scenario, not shown, the local resonant frequency is much higher than the best frequency and plays essentially no role in tuning—in the extreme case, when OCC mass is zero, the resonant frequency is infinity.) For illustration, the two stimulus frequencies are chosen such that the response at the lower frequency, f_1 (*solid curve*) peaks at the place that, if isolated, would resonate at frequency f_2 ($X_{BF1} = X_{RF2}$). The response to the higher frequency stimulus, f_2 (*shaded curve*), peaks at the more basal location (X_{BF2}) but continues on, almost but not quite reaching the position of its own resonant frequency (X_{RF2}). Without damping, the response to frequency f_2 would just reach X_{RF2}, where its wavelength would be zero and size infinitely large. In the presence of damping, when stimulating at frequency greater than or equal to f_2 at the position X_{RF2}, the response would be zero. In experiments such a limiting behavior is not observed because the response amplitude and phase reach a plateau (*dotted horizontal lines* in *upper figure* and *vertical lines* in *lower*) due to the emergence of an evanescent-fast response. The lower curve, oriented at 90°, shows the frequency response at just one location ($X_{BF1} = X_{RF2}$), which is the actual format of the data.

that include active cochlear mechanics (7,8) also exclude significant OCC mass (Lim and Steele used a mass of 0.0015 g/cm^2 at BF = 10 kHz for their chinchilla model, which corresponds to the BM height (9), and Wen used a mass of 0.003 g/cm^2 at BF = 2 kHz in her cat model).

However, other models (1,10) explicitly include mass and the concept of local resonance: the basic mechanism for passive tuning is similar to what was described above for the nonresonant tuning, with the wave slowing and growing as the stiffness decreases. The inclusion of OCC mass makes the OCC's effective-stiffness decrease with frequency and equal to zero at the resonant frequency of a given position. The wave (oscillating at the stimulus frequency) peaks at its best frequency place and stops at the resonance place. In reality, due to damping, the wave will not quite reach its resonant position. The influence of the local resonance is to enhance the slowing and growing of the wave. Lighthill (1) noted this was a case of critical-layer absorption characterized by three points:

1. No wave energy at frequencies above the resonant frequency can pass the point of resonance.
2. There is a decrease of the wavelength as the point of resonance is approached, accompanied by a decrease of the wave speed.
3. Therefore, the wave energy flow is retarded so much that even light damping has enough time to dissipate that energy: the resonance absorbs energy.

Lighthill used this concept to explain the steep apical cutoff in amplitude and accompanying rapid phase variations of passive cochlear tuning as the point of resonance is approached. The resonant frequency of a given location, f_r, depends on the local properties of the OCC (local stiffness, S, and mass, m_{occ}): $2\pi f_r = \sqrt{S/m_{occ}}$. If the OCC mass is zero, the resonant frequency is infinite. Our methodology allows us to find the stiffness and the size of the OCC mass that is playing a role in the mechanics, and thus to calculate f_r. If f_r is less than twice the passive BF, we will say that the OCC mass is significant, and local resonance plays a substantial role in producing the tuning. A smaller mass (giving a resonant frequency larger than two times the BF) will be used to indicate that the tuning is not based on local resonance. The factor two is an arbitrary number, but our experimental results will illustrate that it is a reasonable choice for separation.

In summary, we are left with a class of models that argues that OCC mass is not important to tuning, and another class that argues that it is, through the mechanical effects of the wave approaching (while not reaching) the local resonance position. Despite the centrality of the issue, whether or not OCC mass is critical to cochlear tuning remains an open question of cochlear mechanics. We explore this question through quantitative analysis of the wavenumber, k. The wavenumber is the derivative of phase with distance. In a

sinusoidal wave, k is proportional to the inverse wavelength, $k = 2\pi/\lambda$. The slowing of the traveling wave is reflected in its decreasing wavelength (increasing k) (Fig. 1 *A*). Our goal is to observe k's variation with frequency, coupled to 3D cochlear modeling predictions, to determine whether or not the mechanical response relies upon the presence of significant OCC mass. If the response peak is produced by local resonance, the BF will be lower than, but fairly close to, the local resonant frequency (less than a factor of two), as indicated in the amplitude curves in Fig. 1 *B* (for now ignoring the *dotted lines*). Through the BF region, k will grow very rapidly with frequency, due to the pronounced slowing of the wave—this is apparent in the changing phase slope in Fig. 1 *B*. In contrast, if the response peak is not produced by resonance, k will not grow as steeply in the region of the BF as illustrated later in the article (Fig. 5).

Interferometric measurements were used to map the motion of the basilar membrane under pure tone stimulation in the basal region of the cochlea. The local wavenumber of the traveling wave was found experimentally by taking the difference in phase measured at two adjacent longitudinal positions (separated by distances of tens of micrometers) and dividing by the distance between the two points. The amplitude of cochlear tuning is known to vary greatly with cochlear condition and/or stimulus level via the action of the cochlear amplifier; in contrast, the phase is affected relatively little. Therefore, the cochlear traveling wave and the wavenumber that describes its local wavelength are properties of the passive mechanics. (Relatively small changes in phase related to cochlear nonlinearity do occur (11).) The observation that the phase is little affected by cochlear condition imposes strong constraints on cochlear models (10) and gives us an experimental advantage, as we can do measurements on cochleae that are passive or nearly passive (broad amplitude response at low sound pressure levels along with high compound action potential, i.e., CAP, thresholds) and still gather meaningful phase data. Our measured wavenumber was compared to theoretical results obtained from a 3D model developed by de Boer and van Bienema (12), and the following question was asked: Does the measured wavenumber look more like the model prediction with or without significant OCC mass?

Additional background: fast, slow, and evanescent waves

The excitation of the cochlea by the stapes produces a dual-mode pressure response composed of a pressure difference across the organ of Corti summed with a compressive pressure (sound wave) (13,14). Due to the long wavelengths of sound compared to the cochlea, the compressive wave has almost no spatial variation, constant amplitude along the scalae, and because the compressibility of cochlear structures is high (like that of water), there is negligible motion response of the basilar membrane to the compressive pressure. The compressive pressure is called a fast wave, because it responds in phase with the stapes, with essentially no delay (the speed of sound in water is ~1500 m/s). The pressure difference mode causes the flexible organ of Corti complex to respond elastically. This response launches the traveling wave. In addition to the traveling wave, the pressure difference is associated with nontraveling evanescent-waves in the region of the round and oval windows (or an unnatural window—for example, one drilled for observation (15)). Like the compressive pressure, these are fast modes in that they are in phase with the stapes motion. Unlike the compressive pressure, they cause significant motion of cochlear fluids and tissues. The evanescent-waves diminish rapidly in space and are usually much smaller than the traveling wave, but in the region of the windows they can be substantial, and they are apparent in the data. Measuring at a fixed position with increasing frequency, there comes a point where both the amplitude and phase reach an evanescent-wave plateau. In the schematic of Fig. 1 *B*, this is indicated in the dotted lines that extend horizontally in the upper part of the figure (vertically in the lower), thus truncating the detection of the traveling wave response. The transition to a dominantly evanescent-wave response occurs at a frequency ~1.4–2 times higher than the passive BF in our measurements. Because our analysis uses the phase variations of the traveling wave, it is restricted to frequencies below the plateau.

EXPERIMENTAL METHODS

Animal preparation

Measurements were performed in gerbils, 50–70 g in mass. The care and use of animals were approved by the Institutional Animal Care and Use Committee of Columbia University. The animal was first sedated with ketamine (40 mg/kg) and then deeply anesthetized with sodium pentobarbital (initial dose, 60 mg/kg; supplemental doses, 10 mg/kg when a toe pinch response was elicited) and overdosed with anesthetic at the end of the experiment. The body temperature was maintained at 37°C using an animal blanket. The animal head was firmly attached to a head holder using dental cement. In some cases the head holder was heated by running current through resistive wire wrapped around the head holder. Surgery was performed to expose the left cochlea. First, the pinna was removed. A tracheotomy was made to maintain a clear airway. A small plastic tube of similar diameter as the ear canal (EC) entrance was cemented to the ear canal to couple the speaker and the microphone. The bulla was widely opened to view the cochlea. For the very basal view of the BM, the round window membrane (RWM, which is very transparent) was kept intact whereas for a more apical view of the first turn, the round window opening was enlarged and a portion of the RWM removed. For the latter preparation a glass coverslip closed the opening (no seal was necessary). Its use helped to stabilize the level of liquid inside the cochlea.

Experimental protocol

Basilar membrane vibration upon sound stimulation was measured at different longitudinal positions along the membrane. Experiments were performed in vivo. The CAP response of the auditory nerve to tone pips was measured with an electrode at the round window after opening the bulla and again after several steps of the surgery. It was used to evaluate the hearing capability of the animal, and to identify damage due to the invasive surgery

(16). The cochlear condition was compromised due to the relatively wide opening of the bulla and the enlarging of the round window, resulting in passive (linear) or nearly passive preparations (30–40 dB increase in CAP thresholds in the frequency region of interest at the end of the surgery). The in vivo condition was nevertheless important to maintain the fluid level and passive cochlear condition over several hours of recording (usually, the surgery starts at 9 AM and the experiment ends at ~8 PM).

A RadioShack speaker (Fort Worth, TX) connected to the ear canal of the gerbil was used to deliver pure tones of frequencies from 250 Hz to 50 kHz. A probe tube attached to a B&K microphone (17) (Brüel & Kjær, Naerum, Denmark) was inserted ~1 mm into the EC to perform the sound stimulus calibration. When analyzing the EC data, a probe tube correction was used. Basilar membrane vibrations were measured using a heterodyne laser interferometer coupled to a confocal microscope. The setup has been described previously (18,19). The laser has been changed to a 25 mW semiconductor laser, with wavelength like that of the previous HeNe laser (638 nm), but with a more powerful beam. The phase of the interferometric measurements was corrected for a 14 μs demodulation delay, determined experimentally (20). The BM was viewed using either a 10 or 20× objective lens. The optical sectioning capability of our system allows us to measure BM vibrations without beads through the RWM. For the basal position, in which the BM was viewed through the RWM, the RWM is a potential source of competing signal. However, measurements performed at the same longitudinal position with first the BM and then the RWM in focus showed that independent measurements of each surface could be made (21,22). Measurements of stapes vibrations were also performed with the laser beam focused on the posterior crus.

We show results from two animals, for which the view was such that several longitudinal measurements could be made. Seven other animals showed similar results. Because of the linear nature of the preparations, we emphasize data collected at the relatively high stimulus level of 80 dB SPL.

BACKGROUND TO COCHLEAR THEORY

To determine whether the OCC mass plays a significant role in cochlear frequency selectivity, we compared measurements of the variation of wavenumber with frequency to modeling predictions with and without OCC mass. Below we motivate this analysis by reviewing the equations that govern the motion of the OCC and lead to the dispersion relation. The dispersion relation is the mathematical relationship between the local (at a particular longitudinal location) wavenumber, the frequency, the cochlear dimensions, and the local properties of the OCC—stiffness, mass, and resistance.

The local equations

This work focuses on passive, linear cochlear mechanics and no active forces are considered. We consider responses to pure tone stimulation. The analysis models a cross section of the organ of Corti complex. The pressures adjacent to the OCC (P_{ST} in scala tympani and P_{SV} in scala vestibuli) drive the motion of the fluid on either side of the OCC and the local pressure difference across the OCC, ($P_{SV} - P_{ST}$), drives the motion of the OCC (see Fig. 6 in (23) for an illustration of the forces applied to the organ of Corti). In a symmetric cochlear model, pressures and motions can be separated into symmetric and antisymmetric modes (14). The symmetric mode, in which the pressures in the scalae tympani and vestibuli are equal, is the compressive fast pressure wave. As noted in the Introduction, this does not drive significant OCC motion and we do not consider it further. In the antisymmetric mode, the pressures and the fluid disturbances above and below the OCC are equal in magnitude but opposite in sign, i.e., $P_{ST} = -P_{SV}$. This simplifies the problem to that of a single fluid chamber with a flexible membrane (the OCC) forming one boundary. Almost all cochlear models use this approximation, including the one on which we base our theoretical comparison. The antisymmetric mode actually comprises several modes, both traveling (slow wave) and nontraveling (evanescent-fast wave), as introduced above. While many models are simplified to exclude the evanescent modes, others (3,24) have noted that these modes are necessary to match the boundary conditions in the region of the windows. Our quantitative analysis below only includes the traveling wave, but the evanescent-fast wave influences our results, as will be discussed further below.

The OCC mechanics are described by

$$Z_{\mathrm{occ}} = i\omega m_{\mathrm{occ}} + \frac{S}{i\omega} + R = \frac{(P_{\mathrm{SV}} - P_{\mathrm{ST}})}{v_z} = \frac{-2P_{\mathrm{ST}}}{v_z}. \qquad (1)$$

Z_{occ} is the specific acoustic impedance of the OCC (pressure/velocity), which can be expressed simply in terms of OCC stiffness (S), mass (m_{occ}), and resistance (R). In fact, we will neglect the resistance for most of our analysis because it does not have much effect on the phase unless it is very large. The value v_z is the vertical velocity of the OCC. To model the stiffness of biological tissue as a single, frequency-independent number is a simplification (25,26) and in the discussion we will address whether and how a more realistic, frequency-dependent stiffness would modify our findings. The units of Z_{occ} are dyne s/cm^3. Note that because the driving load is pressure rather than force, the units of mass, stiffness, and resistance are normalized to the area of a BM segment (radial width times a unit longitudinal distance of the BM). To relate to our usual notions of mass and stiffness: the area-normalized mass can be roughly thought of as the height of the OCC that moves as a unit (that is not deformed by penetrating fluid pressure) times its density (similar to that of water); the area-normalized stiffness is the pressure divided by the vertical OCC displacement. (The model stiffness is related to previously measured point stiffness, N/m, via a beam model in Appendix A.)

P_{ST} is the pressure just at the boundary of the BM that drives the motion of the adjacent fluid in scala tympani. Approximating the fluid forces as linear and inviscid (27), we can write

$$P_{\mathrm{ST}} = \rho a_z h_{\mathrm{eq}} = i\omega\rho v_z h_{\mathrm{eq}} = i\omega v_z m_{\mathrm{fluid}}/2, \qquad (2)$$

with $m_{\mathrm{fluid}} = 2\rho h_{\mathrm{eq}}$, the effective fluid mass per unit area (in g/cm^2). The value ρ is the fluid density and a_z is the acceleration of the fluid at the OCC boundary ($a_z = i\omega v_z$). The expression for h_{eq}, the equivalent height of the fluid (given below), embodies the basic fluid physics. It is a

function of the wavenumber and depends on the dimensionality of the model and the geometry of the cochlea (scalae size, BM width). Equivalent height is sometimes identified as Q (12). To provide some insight into h_{eq}, in Appendix B we review how to find it in the relatively simpler one- and two-dimensional cochlear models. (Including fluid viscosity results in an imaginary component of h_{eq}, a minor modification that we do not include.)

From Eqs. 1 and 2 we have the following relation at the boundary of the BM ($z = 0$):

$$i\omega m_{fluid} = -Z_{occ}, \text{ so } \omega^2 m_{fluid} = S - \omega^2 m_{occ} + Ri\omega. \quad (3)$$

Equation 3 describes the relation between the frequency, the fluid mass and the properties of the OCC cross section at a position x. Including the mass of the organ of Corti (m_{occ}) will decrease the effective stiffness of the OCC from S (if $m_{occ} = 0$) to $S' = S - \omega^2 m_{occ}$. Wave speed increases with stiffness; thus we can already see that the effect of m_{occ} is to decrease the wave speed. The value m_{fluid} is a function of the wavenumber of the traveling wave, and this functional dependence will be used to recast Eq. 3 as a dispersion relationship—the relationship between wavenumber and frequency.

Several authors have noted that 3D treatments are necessary for detailed comparison to experimental results (1,3,10). Therefore, to compare with accuracy our experimental results to predictions, we will only consider a 3D model.

Fluid mass in a 3D model

To find the dispersion relation, we need to express m_{fluid} in terms of the wavenumber. For this, we use the 3D model developed by de Boer (28). The model has the form of a rectangular box. The structure contains two symmetric scalae (h = height, b = width, and they are taken to be equal, $h = b$). The OCC occupies a fraction (ε) of the width of the scala. The structure is considered to be infinitely long. The scalae are filled with an inviscid, linear, and incompressible fluid. The OCC is assumed to move linearly and to be described completely by its specific acoustic impedance, Z_{occ}. In view of the linearity and pure tone stimulation, the system response varies with time as $e^{i\omega t}$. The boundary conditions are 1), at the outer walls, the normal component of the fluid velocity is zero; 2), the cochlear windows are driven by an equal and opposite velocity; 3), the pressure goes to zero at longitudinal locations away from the peak; and 4), the boundary condition at both radial edges of the BM are hinged, meaning the second spatial derivative is zero there.

Details about how to find the analytic expression for Q are in de Boer (28); here we simply give the result:

$$Q_{3D}(k) = \frac{\varepsilon}{k\tanh(kh)} + \frac{\pi}{2}\sum_{n=1}^{\infty}\frac{4\varepsilon\cos(n\pi\varepsilon)}{\pi(1-4n^2\varepsilon^2)}\frac{\sin(n\pi\varepsilon)}{(n\pi\varepsilon)}\frac{1}{p\tanh(ph)}$$

$$\text{with } p = \sqrt{k^2 + \frac{4\pi^2 n^2}{h^2}}. \quad (4)$$

The sum is performed over n, an integer that distinguishes the various modes of the fluid waves. de Boer and van Bienema (12) introduced an approximate form of Eq. 4 that simplifies its analytical use:

$$Q_{3D}(k) = \frac{\varepsilon}{hk^2}\frac{1 + b_0 k^2 h^2}{1 + \varepsilon b_0 kh}. \quad (5)$$

The value b_0 is determined by best-fitting plots of Eq. 5 to Eq. 4. Equation 5 is not symmetric for a sign inversion of k, so it treats forward- and backward-going waves differently. Therefore, de Boer later gave a new approximation using a symmetrical analytic expression (29). However, for our purposes the important thing is that the analytic expression has the same shape as the expression it approximates for positive k, and for that Eq. 5 is adequate, and simpler. (We treat passive mechanics, for which any backward going wave is expected to be insignificant.)

Dispersion relation

The dispersion relation is obtained by inserting $Q_{3D}(k) = h_{eq} = m_{fluid}/2\rho$ from Eq. 5 into Eq. 3:

$$k^3 + k^2\left(\frac{1}{\varepsilon b_0 h} + i\frac{2\omega\rho}{Z_{occ}(x)}\right) + i\frac{2\omega\rho}{b_0 h^2 Z_{occ}(x)} = 0. \quad (6)$$

Equation 6 can be solved analytically. By substituting in values for the mechanical elements comprising $Z_{occ}(x)$, the variation of the local wavenumber k with frequency can be studied. Because this is a cubic function for k, there are three roots. One of the roots is real in the absence of OCC damping, and positive. The other two roots have negative real parts and imaginary components even in the absence of OCC damping. The first root represents the forward traveling wave solution. When damping is included in Z_{occ} this root has an imaginary part. The real part of k conveys the phase of the response and the imaginary part conveys the decreasing amplitude due to resistance. The real part of this theoretical k was used to compare with the k derived via the experimental phase, k_{exp}.

We checked the validity of our experimental/theoretical comparison by programming a two-dimensional (2D) cochlear computer model (5). Using this model we compared the experimental wavenumber k_{exp} (as calculated from the difference in velocity phase at two adjacent longitudinal locations, divided by the distance between these locations) with the model's actual k_{2D} values ($k_{2D} = -2_{i\omega\rho}/Z_{occ}$; see Appendix B). In this test case a departure between the experimental and theoretical k values did appear, but only for a very large value of OCC resistance. The departure arose because with the inclusion of OCC resistance, the OCC impedance has both real and imaginary parts, resulting in a frequency-dependent phase-shift of velocity that appeared in the experimental k_{exp} but not in the theoretical k_{2D}. This

introduces a small additional (<90°) frequency-dependent phase variation.

Parameter values

In Eq. 6, the parameters corresponding to the geometry of the gerbil cochlea at our one turn measurement position (~2 mm away from the round window) were determined using Plassmann et al. (30). The dimensions of the scalae were estimated as follows: the height was taken equal to the width of each scala ($h = b = 550$ μm), and the BM occupied a fraction $\varepsilon = 0.3$ of the total width, which corresponds to a BM width of 165 μm, to model the basal BM. The value ρ is the fluid density, taken as that of water, 1 g/cm^3. The parameter b_0 was chosen for the best correspondence between the analytical expression for $Q_{3D}(k)$ in Eq. 4 and its approximation in Eq. 5: $b_0 = 1.2$. The match is shown in Fig. 2, and one- and two-dimensional approximations for Q (as derived in Appendix B) are included for comparison. Finally, the only free parameters were the components of $Z_{occ}(x)$: stiffness (S), mass (m_{occ}), and damping (R). Stiffness and mass can be recast as resonant frequency,

$$f_r = \frac{1}{2\pi}\sqrt{\frac{S}{m_{occ}}}.$$

As presented in the Introduction, f_r (the frequency at which the wave stops) must be greater than the BF (the frequency at which the wave peaks); the question is how much greater. In addition, as discussed in Background to Cochlear Theory, because (experimentally) the traveling wave dominates the evanescent wave up to the evanescent-wave plateau, and (theoretically) the traveling wave stops when its frequency reaches f_r, f_r must also be greater than the frequency where the plateau just begins. If m_{occ} is not important, f_r will be much higher than the BF—substantially greater than a factor of two, an arbitrary but reasonable number that is based on our experimental results. If m_{occ} is important (if local resonance has a significant role in slowing the wave), f_r will be fairly close to the BF—less than a factor of two. The plots below illustrate this division.

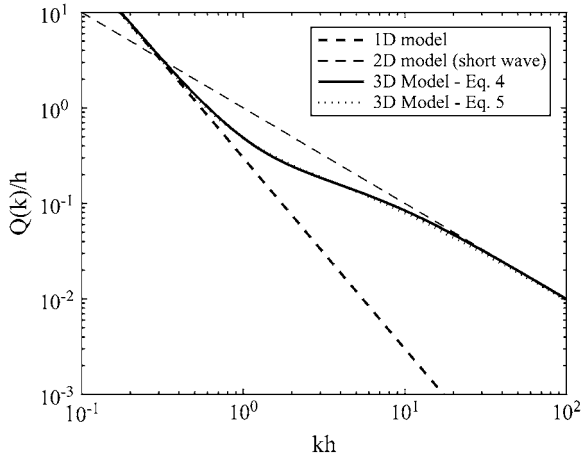

FIGURE 2 The analytical expression for the equivalent mass, Q_{3D}, given by Eq. 4 is compared to its approximation in Eq. 5. Parameters used were the following: $h = b = 550$ μm; the BM occupied a fraction $\varepsilon = 0.3$ of the total width, and $b_0 = 1.2$. The Q function for a 1D model, $Q_{1D} = \varepsilon/(hk^2)$ and a 2D model, $Q_{2D} = 1/k$ (short-wave approximation) are included for comparison.

EXPERIMENTAL VERSUS THEORETICAL RESULTS

Results from two experiments are presented and compared to theoretical results. These are in vivo passive-cochlea measurements, at a stimulus level of 80 dB SPL.

Basilar membrane response at several nearby longitudinal locations (Exp#18)

Fig. 3 illustrates the BM velocity at a basal region characterized by a passive BF of 35–40 kHz viewed through the intact RWM. Vibrations of the bony round window opening were measured and defined our background level (~−60 dB re 1 mm/s at all frequencies). As we moved the measurement location from more basal to more apical (R#24 to R#27), the BM velocity amplitude peaked at lower frequencies and the phase shifted so that the rapidly downward sloping part started at lower frequencies. The observed shift in BF is as expected for the 315 μm longitudinal distance between R#27 and R#24, based on the gerbil cochlear map (31). The longitudinal distance between measurement positions was found as $d = \sqrt{\Delta x^2 + \Delta y^2 + \Delta z^2}$, where the coordinates at each position were read from our linear positioning system. (Note that the plane of the BM was not perpendicular to our viewing/measuring axis; there is a substantial change in z coordinate as well as x and y coordinates between points, reported in the figure caption. Thus, we measured the BM velocity with a significant angle relative to the axis that is perpendicular to the plane of the BM. This is not expected to influence the phase measurement that is our emphasis.) The four amplitude and phase responses show differences over the range 25–50 kHz but overlap at low frequencies. This behavior was also observed by others (32,33).

The total recording time for this experiment was 6 h. The preparation needed to be stable in time to make the analysis meaningful. Fig. 4 shows the responses measured at the same position on the BM, but at different times: R#20 was measured 35 min after and R#25 was measured 65 min after R#14. Recording positions (x, y, and z) were adjusted to maximize the carrier level (signal proportional to the amount of light that reached the photodetector) at a position very close to the reference point (R#14), and actually differed from it by 11 and 19 μm. Amplitude responses for the three curves were similar and the phase responses overlapped precisely.

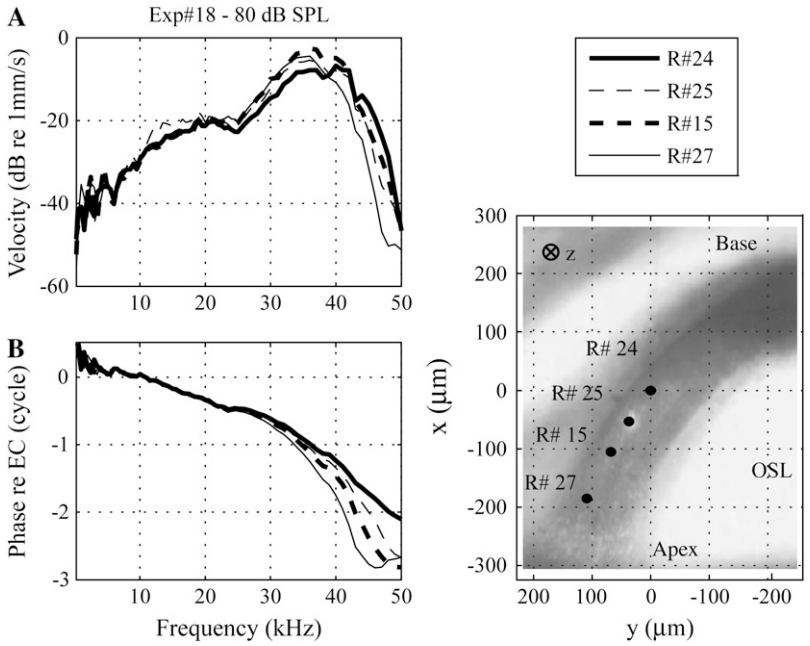

FIGURE 3 In vivo, passive measurements of velocity amplitude (*A*) and phase (*B*) at four longitudinal positions along the BM (Exp#18) from base to apex: R# 24, 25, 15, and 27. The recording positions are illustrated in the picture (*BM*, darker band; *OSL*, osseous spiral lamina). The coordinates were set to ($x = 0$, $y = 0$, $z = 0$) for R#24. Position of each of the runs was recorded (in μm): R#25 (-53, 37, 87), R#15 (-105, 68, 157), and R#27 (-185, 109, 231).

Experimental versus theoretical wavenumber variations (Exp#18)

The wavenumber was found by taking the difference in the phase (in radians) of two closely spaced locations and dividing by the longitudinal distance between these locations, $k_{exp} = \Delta\varphi/d$. k_{exp} is the wavenumber midway between the two measurement positions. (Note that this definition of k_{exp} is valid only at frequencies where the traveling wave is dominant, as will be discussed further below.) Fig. 5 compares experimental variation of the wavenumber as a function of stimulus frequency obtained using R#24 and 25 (*line* with *dots*) to theoretical ones obtained by solving Eq. 6 for k. The influence of the parameters of the model (OCC mass, stiffness, and resistance) on k is studied.

Fig. 5 *A* shows the variation of k_{exp}. As expected, k_{exp} increased as the frequency approached the best frequency, BF $\sim$38 kHz (i.e., as the wave approached the best place). The variations of k_{exp} are noisy below 5 kHz; the phase responses of both runs are similar and not smooth (but above the noise floor), therefore small differences in phase are enhanced. With the 10$\times$ objective lens used during this experiment a relatively high carrier level was obtained over a distance of ± 10 μm along the z axis from the position where the carrier level was maximum. Because the z-position of one measurement point is chosen by the maximum carrier level in combination with an in-focus view, a spread in z-positioning of ± 10 μm can occur and introduces uncertainty into the measured d. The error bars in Fig. 5 *A* illustrate how the uncertainty in separation distance affects k_{exp}. The influence is small enough that it will not affect our conclusions.

In Fig. 5 *B*, the OCC impedance was considered as a stiffness with and then without OCC mass. Including OCC mass changed the shape of the curve. When the OCC was a pure stiffness, k was slightly bigger than k_{exp} below 38 kHz and was much too small at high frequencies (*dotted line*). Attempting to fit the data with a smaller stiffness value (without mass), the too-big/too-small frequency transition shifts up in frequency (*dashed line*), and the fit in the lower frequency region is not at all close. To model the slow growth in k at low frequencies followed by rapid growth at high frequencies (above BF, indicated by the *asterisk*), including substantial OCC mass was necessary (*solid line*).

Adding resistance did not influence k unless the OCC resistance was so big that its impedance rivaled the impedance of the effective stiffness $S' = S - \omega^2 m_{occ}$ (Fig. 5 *C*). The effect of resistance was to reduce k; therefore including resistance emphasized the need for mass to explain the experimental data. For example, with $R = 1500$ g/s cm^2, we needed a bigger mass (0.05 instead of 0.025 g/cm^2), a smaller resonant frequency (47 instead of 53 kHz) resulting in a bigger stiffness (4.36 instead of 2.77 10^9 dyn/cm^3) to fit the experimental data. This value for the resonant frequency was not realistic, as then the wave would not exist at frequencies above 47 kHz, which was not the case; in Fig. 3, amplitude and phase responses of R#24 and 25 remained in a traveling wave mode above 47 kHz. Here the resistance is taken constant with frequency. This is a rough approximation, as R has been measured and showed a decrease followed by an increase with frequency (13,34). Because the effect of resistance on k is small compared to the dramatic effect of mass, and to reduce the parameter space, we do not consider resistance further.

Fig. 5 *D* explores the sensitivity of the theoretical curves to changes in stiffness and mass parameters. All the curves in this figure were obtained with the stiffness, $S = (2\pi f_r)^2 m_{occ}$,

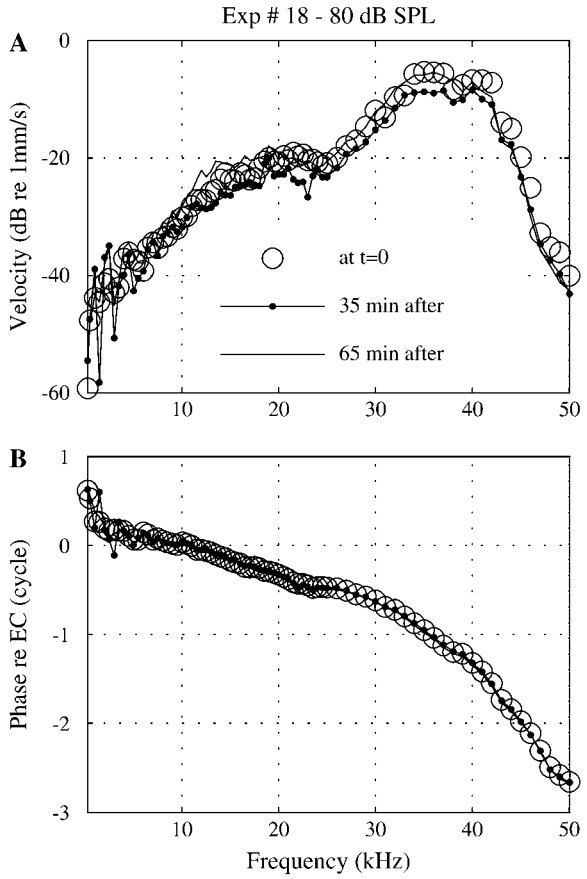

FIGURE 4 Demonstration of measurement stability over time: velocity amplitude (*A*) and phase (*B*) measured at approximately the same position on the BM at different times: At $t = 0$, R#14 (−49, 38, 97); $t = 35$ min R#20 (−51, 53, 85), and $t = 65$ min R#25 (−53, 37, 87).

calculated with $R = 0$, a fixed resonant frequency of 53 kHz (same as Fig. 5 *B*), and a varying mass (0.015, 0.025, and 0.035 g/cm^2). With lower S and m_{occ}, k was bigger. This is easily understood: because f_r is fixed, and $R = 0$, all the curves must approach the vertical at 53 kHz. At frequencies much lower than f_r, k is not much influenced by m_{occ}, and is determined solely by the fluid (whose properties are fixed) and the stiffness. The smaller stiffness results in a slower wave, thus a shorter wavelength and a larger k. Even as f_r is approached and m_{occ} becomes influential this tendency remains.

Based on the experimental/theoretical comparisons in Fig. 5, *B* and *D*, the resonant frequency for the location with passive BF of 38 kHz was 53 kHz, a factor of 1.4 greater than the BF. Thus, significant OCC mass was necessary to produce the pronounced increase in k slope—in other words, an approach to the local resonant frequency appears to influence the response substantially. It might be argued that up to the BF ~38 kHz, the theoretical k with and without OCC mass are very close and both fit the experimental k, and therefore that the OCC mass is not important to passive peaking. However, the behavior on the high frequency side of the peak is an important element of peaking. To make the point: if the high frequency side amplitude did not come down, there would be no peak. Therefore, the rapid increase in phase and k with frequency is linked to the high frequency side decrease in amplitude even in the passive case—as described by the theory of critical layer absorption.

Fig. 6 assembles curves of $k(f)$ from three longitudinal locations along the basal turn of the BM. The relative position of each run is in the inset. Experimental (*lines* with *symbols*) curves are compared to the theoretical (*thin lines*) curves that provided the best fit. For these data, as in Fig. 5, best fits were obtained when significant OCC mass was included. Considering both parameters (mass and stiffness) as free, good fits were obtained with a decreasing stiffness (from 3.2 10^9 to 1.7 10^9 dyn/cm^3—factor of 1.88) and a decreasing mass (from 0.03 to 0.019 g/cm^2—factor of 1.58) from the more basal to the more apical position. This decrease in mass was not expected, and the fitting was redone with the mass taken as constant ($m_{occ} = 0.022$ g/cm^2). The fits are still very good with the constrained mass value and stiffness values ranging from $S = 2.53\ 10^9$ to $2\ 10^9$ dyn/cm^3 (Fig. 6). With a smaller OCC mass (0.015 g/cm^2)—closer to what the anatomy predicts—the fits were less good but still reasonable.

The definition of the wavenumber $k_{exp} = \Delta\varphi/d$ is valid only over a frequency region where the traveling wave dominates. As soon as one of the phase responses reaches or approaches the plateau region, which likely signals that the BM is responding primarily to the evanescent-fast wave (1,35,36), k_{exp} can no longer be calculated. That is why above a certain frequency—48 kHz for k_{exp} (24,25), 46 kHz for k_{exp} (25,15), and 43 kHz for k_{exp} (15,27)—the variation of the wavenumber changes its trajectory.

More results from the first turn of the gerbil cochlea, slightly further apical

Results from another experiment (#8) are in Fig. 7. The view of the BM was of turn one, corresponding to a region where BF = 20–25 kHz. To access this region, the RWM was removed and the resulting opening was covered with a glass coverslip, which was simply positioned on the bony opening without sealing. BM vibrations were recorded over a total distance of 285 μm along the longitudinal axis of the BM. Run #20 corresponds to a more basal, R#19 to a more apical position. The phase responses show the expected shift in frequency (Fig. 7 *B*). The shift in amplitude is small, likely due to the passive condition with a relatively broad response (Fig. 7 *A*). Background vibrations were measured with the laser beam focused on the bone around the oval window and were less than −60 dB re 1 mm/s at all frequencies. The repeatability of the measurements was checked by recording the same position with a 2 h time separation. Fig. 7 *C* compares k_{exp} (*lines* with *symbols*) to the theoretical k with (*solid lines*) and without (*dashed lines*) OCC mass. Best fits were obtained including a significant m_{occ} of 0.015 g/cm^2

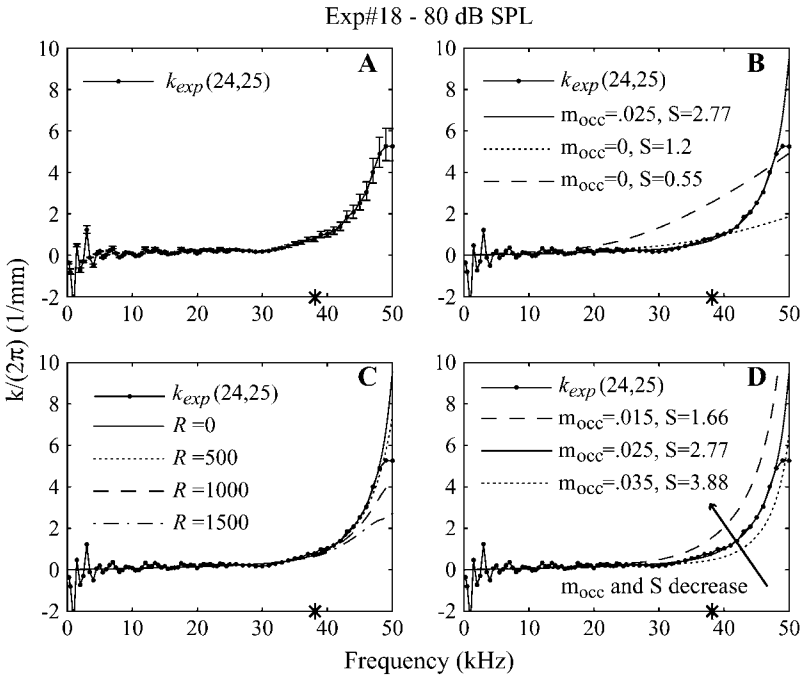

FIGURE 5 In the four panels, the curve with dots represents the variation of k_{exp} with frequency obtained from the phase responses for R#24 and 25 ($d = 108$ μm). The asterisk in the x axis represents the BF position (~38 kHz). (*A*) The error bars illustrate how an uncertainty of ± 10 μm in the z-coordinate can affect k_{exp}. (*B*) Comparison of experimental to theoretical k with and without OCC mass. The best fit was obtained when a significant m_{occ} was included (*solid line* through *data points*). R was set equal to 0, the resonant frequency to 53 kHz. S values are $\times 10^9$ dyn/cm^3, m_{occ} in g/cm^2. Dashed and dotted lines show that attempted fits with no mass were not successful. (*C*) The effect of resistance was small. The resistance needed to be a substantial fraction of the total OCC impedance to have any effect on k, and its effect was to impair rather than improve the fit. f_r was fixed and set to 53 kHz, $m_{occ} = 0.025$ g/cm^2 and $S = 2.77\ 10^9$ dyn/cm^3 for all. R in dyne s/cm^3. (*D*) Theoretical k obtained with $R = 0$, a fixed resonant frequency, $f_r = 53$ kHz, a varying m_{occ}, and a stiffness determined by $S = (2\pi f_r)^2 m_{occ}$. S values are $\times 10^9$ dyn/cm^3, m_{occ} in g/cm^2. The figure illustrates the sensitivity of the model to stiffness and mass.

(and like above, constrained to be one value for the set). Going from the more basal to a more apical position within this series of measurements, there was a decrease in stiffness, from 5.2 10^8 to 3.9 10^8 dyn/cm^3 (factor of 1.34).

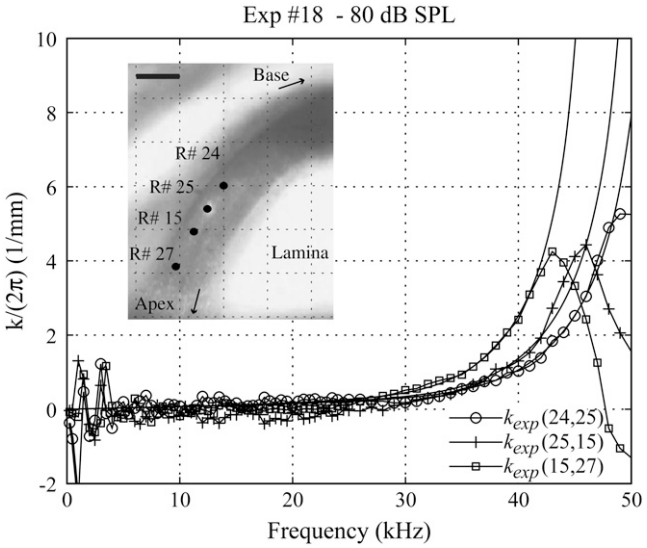

FIGURE 6 Experimental (*lines* with *symbols*) and theoretical (*thin solid lines*) k as a function of frequency. The inset shows the positions of the measurements. The more basal k_{exp} was obtained using the phase responses from R#24 and 25 (*line* with *circles*, $d = 108$ μm) and the more apical position using R#15 and 27 (*line* with *squares*, $d = 116$ μm). k_{exp} using R#25 and 15 (*line* with *plus*, $d = 93$ μm) corresponds to a position between the two others. Theoretical k values were obtained with m_{occ} set to a value of 0.022 g/cm^2. Going from the more basal to the more apical position, there was a decrease in stiffness ($S = 2.53\ 10^9$ dyn/cm^3, then 2.35 10^9 dyn/cm^3 and finally 2 10^9 dyn/cm^3) and a decrease in resonant frequency (54 kHz, 52 kHz, and 48 kHz, respectively). R was set to zero for all. The scale bar is 100 μm.

Results for two animals were presented in this section, but similar results (showing a need for significant OCC mass to fit the data) were obtained with seven other animals: one in the more basal region (Exp# 21: BF ~38 kHz, $m_{occ} = 0.029$ g/cm^2, and $S = 2.6\ 10^9$ dyn/cm^3), four animals in the region BF ~20–24 kHz (Exp# 20-28-29-33: $m_{occ} = 0.0056$–0.0196 g/cm^2 and $S = 3.2$–$9.5\ 10^8$ dyn/cm^3) and two in a region where BF ~ 16–18 kHz (Exp# 17–30: $m_{occ} = 0.004$–0.0093 g/cm^2 and $S = 2$–$3.2\ 10^8$ dyn/cm^3).

MORE DETAILED EXPLORATION OF RESULTS

In this section, we will consider the different factors that can affect the experimental wavenumber and might influence our conclusions. First we will consider the effect of the distance between the two measurement locations (d), then the effect of the evanescent-fast wave on the slope of the phase response. Finally, we will extend the analysis to more data sets, including active preparations and more apical measurements.

Distance between the two locations

The theoretical wavenumber is defined at a longitudinal location, and we approximate this wavenumber via measurements of phase at two flanking longitudinal locations. Based on the definition of the derivative, as the separation between locations becomes larger, the $\Delta\varphi/d$ value becomes a less and less good approximation to the slope at the intermediate point. On the other hand, if the points are too close together, the difference between the phases is overly influenced by random experimental noise. It can be shown analytically that for phase changing more rapidly than quadratically with

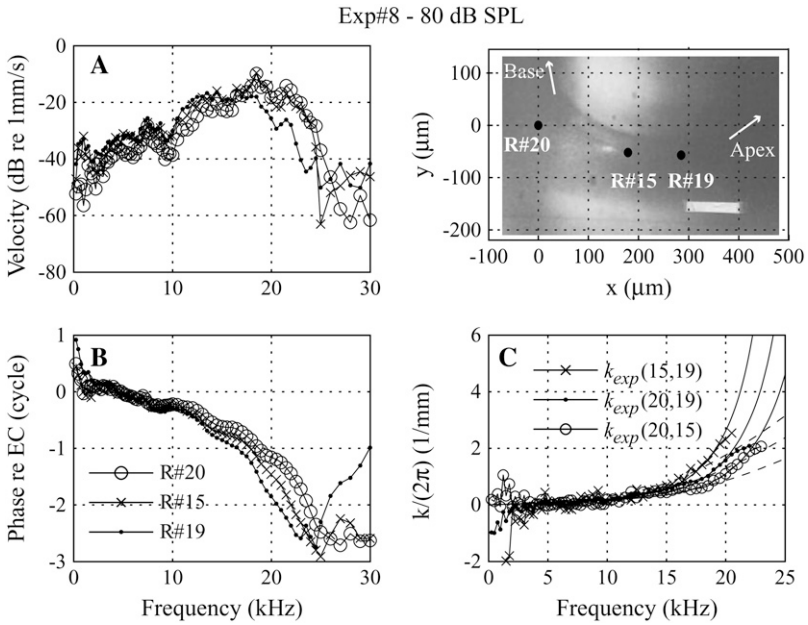

FIGURE 7 BM vibrations were measured at different positions in the first turn of the gerbil cochlea as illustrated in the picture, at a more apical location than in Fig. 3. Velocity amplitude (*A*) and phase (*B*) are shown for three locations. Coordinates were reset to (0,0,0) for R#20. Position of each of the runs was recorded (in μm): R#15 (179, −52, −196) and R#19 (285, −57, −328). The scale bar in the picture is 100 μm. Panel *C* shows k_{exp} values at three positions along the BM (*lines* with *symbols*), compared to theoretical ones with and without OCC mass (*solid lines* and *dashed lines*, respectively). The more basal position is k_{exp} (20,15) with $d = 270$ μm, followed by k_{exp} (20,19) with $d = 438$ μm and the more apical position k_{exp} (15,19) with $d = 169$ μm. The data were only well fit when significant OCC mass was included. A m_{occ} value of 0.015 g/cm^2 provided good fits to all the curves, with a decreasing stiffness from the more basal to the more apical position ($S = 5.2\ 10^8$ dyn/cm^3 and $f_r = 29.5$ kHz; $S = 4.4\ 10^8$ dyn/cm^3; and $f_r = 27.5$ kHz, $S = 3.9\ 10^8$ dyn/cm^3, and $f_r = 25.5$ kHz).

position, the increase in (absolute value of) the slope on the high frequency side of the midpoint (compared to the slope at the midpoint) is greater than the decrease in slope on the low frequency side of the midpoint. So, the phase slope assigned to the midpoint, and therefore k_{exp}, is expected to be erroneously large for large d. This might seem wrong, since in the literature (32,36,37), the largest k_{exp} was found in the experiment where d was smallest (32). This is not inconsistent with the arguments above, however, because at each location the phase can only be found up to a little above that location's BF, where the phase levels off to a plateau value. Therefore, the wavenumber for a point can only be calculated up to about the BF of the more apical of the two points of measurement and as d gets larger and larger, the wavenumber is limited to lower and lower frequencies, further from midpoint's own BF. Because k grows rapidly as BF is approached, the largest k_{exp} is expected to be found when d is small, simply because the midpoint's own BF can be more closely approached. On a related note: the shape of the k curve is relatively flat at low frequencies, then abruptly curves up. We have seen that the abruptness is responsible for the apparent need for significant OCC mass. Increasing d softens this abruptness. Therefore, the more localized the measure of k_{exp} is, the stronger will be the case for significant OCC mass.

Slow wave/fast wave interaction

Wavenumber is based on the phase-versus-frequency response; as a consequence experimental inaccuracies in the measurement of phase would be reflected in the calculation of k_{exp}. The high frequency phase plateau imposes a frequency limit beyond which traveling wave wavenumber cannot be determined. Our interpretation of the plateau is that the traveling wave response has become small enough that the evanescent-fast wave response is dominant. We were concerned that at frequencies below the plateau, but close to it, interference between evanescent wave and traveling wave responses might cause ripples in the phase-versus-frequency curves. Evanescent wave interference in measurements of OCC motion was described by Cooper and Rhode (15). The alternating flattening and steepening of phase caused by interference could lead us to an erroneous conclusion regarding OCC mass. The thick lines in Fig. 8 *A* show the Exp#18 phase responses from runs 15 and 27 previously seen in Fig. 3. These curves are fairly smooth but do show phase ripples in the 35–45 kHz region. To understand how the ripples in phase affect k_{exp}, we smoothed them out (by eye) so the phase followed the center-line shown in the thin lines in Fig. 8 *A*. Fig. 8 *B* contrasts the k calculated using the original (*solid curve*) and smoothed (*shaded curve*) phases, and shows fitted curves from the model (*thin lines*). In the fitted curves the mass of the OCC was reduced from 0.022 to 0.01 g/cm^2 when using the smoothed data. Therefore, the contamination of traveling wave motion with evanescent-wave motion might cause us to overestimate the OCC mass. If so, this helps reconcile the apparent mass decrease as the measurements moved apically (0.022 for Fig. 6 to 0.015 in Fig. 7), as the evanescent-wave influence will diminish with distance from the region of the windows. However, even with the correction for the influence of the evanescent-wave, substantial OCC mass was indicated; the dashed curve is a massless fit and it is much less successful.

Extending the analysis to more data sets

In this study we presented our experimental data from passive preparations, which was justified by the approximate

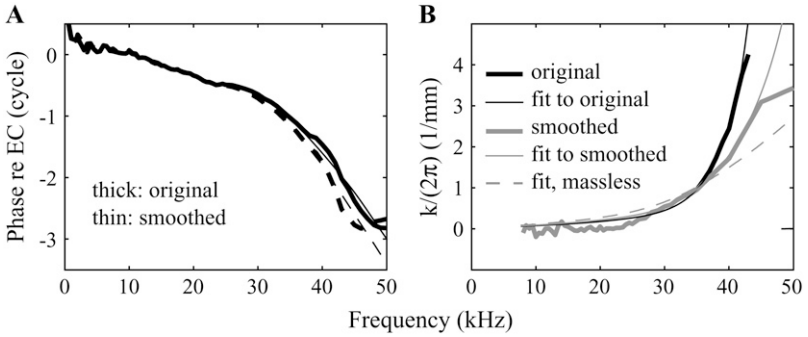

FIGURE 8 (*A*) Experimental phase responses (Exp#18 R#15, *solid bold line*; Exp#18 R#27, *dashed bold line*) and new phase responses after smoothing out the ripples in the phase (*solid* and *dashed thin lines*). (*B*) Corresponding experimental and fitted theoretical k values. The k_{exp} curve plotted with a solid thick line was calculated with the original phase values, the one plotted with a shaded thick line was calculated with the smoothed phase values. Regarding the fitted lines: the black thin line is the fit to the original k_{exp} curve ($m_{occ} = 0.022$ g/cm^2, $S = 2\ 10^9$ dyn/cm^3, and $f_r = 48$ kHz) and the shaded thin line is the fit to the k_{exp} curve from the smoothed phase curves ($m_{occ} = 0.01$ g/cm^2, $S = 2\ 10^9$ dyn/cm^3, and $f_r = 60$ kHz). The theoretical k without mass is also shown (*dashed shaded line*) to illustrate that OCC mass was needed for a good fit.

insensitivity of phase to cochlear condition. However, although phase is not very sensitive to cochlear activity, there are usually small level-dependent variations caused by the active nonlinearity that might be influential in the calculation of $k_{exp}(f)$. Moreover, the results presented have all been from a basal turn of the cochlea. To test how robust our conclusions are—that OCC mass plays a significant role in frequency selectivity in the base, but that this significance wanes toward the apex—we applied the analysis to some in vivo measurements of turn one BM motion in active cochleae from the literature. This allowed us to evaluate the difference that healthy preparations would have on the results, as well as to probe the question of the need for significant OCC mass in regions that were 2.5–3.5 mm away (BF ~12–18 kHz) from the cochlear windows (33,38).

Gerbil basilar membrane vibrations from Cooper (38)

Cooper's results from two gerbils are in Fig. 9: amplitude (*A*) and phase (*B*) from the 12 kHz place at stimulus levels of 50 and 80 dB SPL and from the 18 kHz place at 80 dB SPL. The 12 kHz place phases show the generally observed (11) mild phase steepening of the moderate SPL (active) data compared to the high SPL (closer to passive) data. Closely spaced longitudinal measurements were not part of Cooper's study. To calculate k_{exp} from Cooper's data, we used scaling-symmetry and the gerbil's place-frequency map (31) to generate the phase responses at close-by locations from a single $\varphi(f)$ curve (39). The value k_{exp} was estimated from generated responses separated by $d = 150\ \mu$m.

The $k_{exp}(f)$ derived from Cooper's results are in Fig. 9 *C*. The influence of the BF position is explored first (at 80 dB stimulus level). The thick lines show the curves derived from the data, the dashed thin lines give the best fit of the theoretical $k(f)$ without OCC mass, and the solid thin lines give the best fit where mass was included. As in the results from our data above, including mass gave a much better fit to the data.

Analyzing the phase responses from the lower BF position, we compared k_{exp} for an active (50 dB) to an

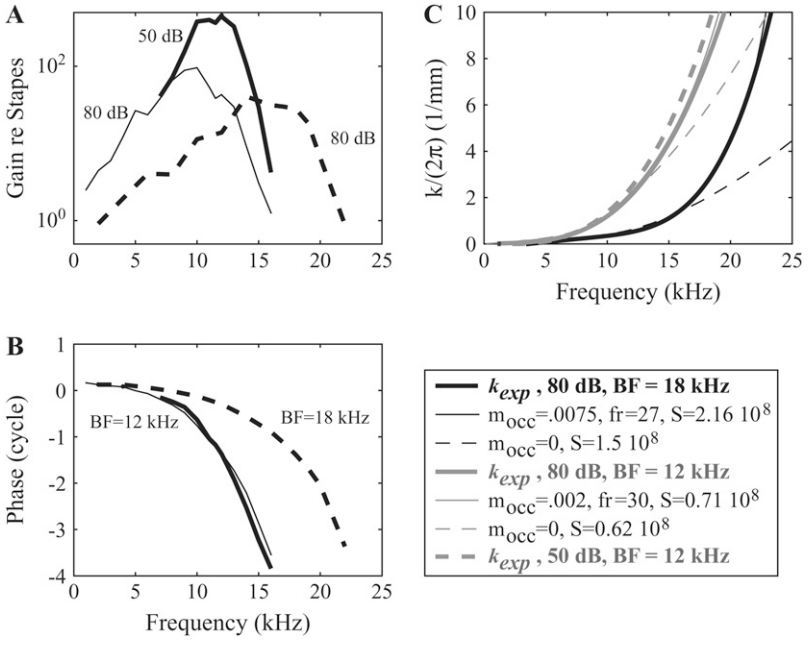

FIGURE 9 BM responses relative to stapes from two active gerbil cochleae, from Cooper (38). Amplitude (*A*) and phase (*B*) of a region with BF = 12 kHz with stimulus levels of 50 (*bold solid line*) and 80 dB SPL (*thin solid line*) and a region with BF = 18 kHz (in a different gerbil) with a stimulus level of 80 dB SPL (*bold dashed line*). (*C*) Corresponding k_{exp} and theoretical k values as noted in legend. Best fits were obtained with OCC mass. There was a decrease of the mass and the stiffness from the more basal (BF = 18 kHz) to the more apical (BF = 12 kHz) position. S values are in dyn/cm^3, m_{occ} in g/cm^2, resonant frequency in kHz, and $R = 0$ for all.

approximately passive (80 dB) preparation. Because the low SPL $\varphi(f)$ curve has a more pronounced flat/steep transition compared to the high SPL phase curve, it is not a surprise that the low SPL $k_{exp}(f)$ curve was similarly flatter/steeper than the high SPL curve (*shaded thick* and *shaded dashed lines* in Fig. 9 *C*). However, the general shape of the curve was unchanged and when compared to the theoretical curves, best fits were obtained when OCC mass was included and the mass was similar between the two ($m_{occ} = 0.0018$ g/cm^2 at 50 dB and $m_{occ} = 0.0020$ g/cm^2 at 80 dB). The small amount of change apparent in the k_{exp} curves could be modeled via OCC resistance change (rather than mass, recall the effect of resistance in Fig. 5 *C*), which is consistent with the idea that the cochlear amplifier acts via changes in resistance, not stiffness (10,34,40).

Chinchilla BM vibrations from Rhode and Recio (33)

Rhode and Recio measured chinchilla basilar membrane motion at several adjacent longitudinal locations, so their results can be used directly to calculate $\Delta\varphi(f)$ and find $k_{exp}(f)$. Their phase results and derived $k_{exp}(f)$ are in Fig. 10. The four sets of phase results (BFs of 7, 7.9, 10.7, and 12.1 kHz) were used to calculate two k_{exp} curves, corresponding to BFs of 7.45 (using the 7 and 7.9 kHz phase data) and 11.4 kHz (using the 10.7 and 12.1 kHz phase data). The distances d were 360 μm and 450 μm. The model dimensions were for gerbil and have not been modified for chinchilla, but a simple application of the analysis to these data reinforces the findings from above. The results were better fit when OCC mass was included in the theoretical expression. The mass was relatively small, and the mass and stiffness values correspond to resonant frequencies of 20 and 25 kHz, more than two times the BFs. The mass used (0.003 g/cm^2) was twice the one used by Lim and Steele (0.0015 g/cm^2) to model the chinchilla BM response at BF = 10 kHz (7). Therefore, while mass does slow down the traveling wave and increase the wavenumber compared to the massless condition, its effect is not pronounced in these results.

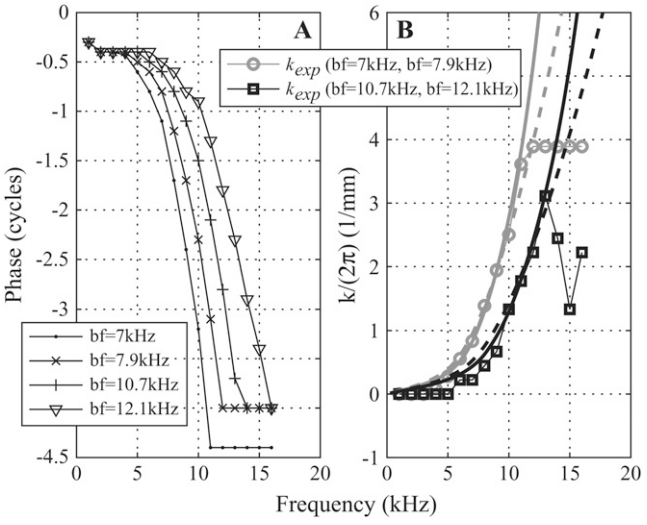

FIGURE 10 The left panel shows the phase responses measured on a single chinchilla BM by Rhode and Recio (33) at four different locations (BF = 7 kHz, 7.9 kHz, 10.7 kHz, and 12.1 kHz). The right panel shows the derived $k_{exp}(f)$ obtained from the phase responses at 7 kHz and 7.9 kHz with $d = 360$ μm (*curve* with *circles*) and from the responses at 10.7 kHz and 12.1 kHz, with $d = 450$ μm (*curve* with *squares*). Experimental curves are compared to the theoretical ones with (*solid lines*) and without mass (*dashed lines*). The parameter values were as follows: lower frequency (*shaded lines*) fit with mass: $m_{occ} = 0.003$ g/cm^2, $f_r = 20$ kHz, $S = 0.47\ 10^8$ dyn/cm^3, and without mass: $S = 0.38\ 10^8$ dyn/cm^3; higher frequency (*black lines*) fit with mass: $m_{occ} = 0.003$ g/cm^2, $f_r = 25$ kHz, and $S = 0.74\ 10^8$ dyn/cm^3, and without mass: $S = 0.58\ 10^8$ dyn/cm^3.

DISCUSSION

Variation of OCC mass in the basal turn of the gerbil cochlea

The mass of the OCC that provided a good fit can be translated to height assuming that the density of the OCC is approximately that of water ($\rho = 1$ g/cm^3). The values can be compared to the anatomical height from unfixed hemicochlea micrographs of Edge et al. (2), in which the gerbil BM thickness decreased from ~55 μm in the basal turn to ~35 μm in the apical turn and the OCC thickness increased from ~125 μm in the basal turn to ~200 μm in the apical turn.

At a measurement position in the basal turn (BF ~35–40 kHz), the predicted OCC height was 220 μm (Fig. 6). When the phase ripples were smoothed out (Fig. 8 *B*), best fit was obtained with a smaller mass (0.01 instead of 0.022 g/cm^2), resulting in a smaller height (100 μm). These values are much greater than the height of the BM, but consistent with the anatomical height of the OCC. This correspondence argues that the entire OCC and enclosed fluid, not just the BM, is the relevant structural element governing cochlear mechanics in the base of the cochlea.

At a more apical position (BF ~20–25 kHz), the m_{occ} necessary was smaller than in the more basal curves of Fig. 6, which was not expected (decrease of the height from 220 to 150 μm in Fig. 7 *C*). Typically in cochlear models OCC mass is either neglected or considered unchanging longitudinally. If it increases apically this helps establish a resonance-based frequency place map and the anatomy does suggest a slight increase apically. Therefore, the apical decrease in mass is hard to reconcile with a resonance-based map.

When extending the study to more data sets, similar results were obtained. In Fig. 9, at the more apical position (BF ~12 kHz), the mass value was smaller than at the more basal one (BF ~18 kHz): from 0.0075 to 0.0020 g/cm^2. In fact, in the analysis of Cooper's data the best fit was obtained with a higher resonant frequency in the more apical than in the more basal position. As above, this indicates that the role of local resonance in tuning diminishes apically.

Taken together, the basal and turn one results suggest that the mechanism for slowing the traveling wave might vary

longitudinally, with OCC mass and the concept of local resonance playing a more prominent role in the most basal regions.

Comparisons with previous studies of OCC stiffness and impedance

In Appendix A, we compare our volumetric stiffness values to point stiffness values from the literature, by analyzing both sets of data with a transverse beam model. The stiffness found in this article was 2–2.5 10^9 dyne/cm^3 at the more basal location (BF ~35–40 kHz) and 3–5 10^8 dyne/cm^3 at the slightly more apical location (BF ~20–25 kHz). After the beam analysis, these values overlap with the point stiffness measurements of Olson and Mountain (41) and Naidu and Mountain (42) and are roughly within an order of magnitude (usually overlap within a factor of five) of those predicted from the Emadi et al. (43) results. This article's method for determining stiffness was based on measurements of wavenumber and a 3D cochlear model, in which stiffness was treated as a free parameter. Therefore, the confirmation provided by the close match with experimental point stiffness values is reassuring.

As a very simple check, the BM displacement at frequencies well below the peak can be related to an approximate value of the driving pressure, to find a rough value of BM stiffness. For example, in Fig. 3, the velocity at 10 kHz corresponds to a displacement, $v/\omega = 50$ nm. The stimulus pressure within the ear canal was 80 dB SPL and at frequencies well beneath the peak, the driving pressure within the cochlea can be approximated using the ~25 dB gain of the gerbil middle ear (44) as ~5 Pa. This gives a specific acoustic stiffness, P/displacement of 10^9 dyne/cm^3, in good agreement with the values above.

Scherer and Gummer (26) did not find a masslike impedance in their point measurements of OCC impedance measured through very high frequencies. However, they were compressing the OCC, not displacing it, so it is not clear what to expect in terms of mass. Previous studies by one of the current authors (13) did find evidence for significant OCC mass—in those measurements the ear was stimulated and both pressure at the OCC and the motion of the BM were measured to determine Z_{occ}, and at frequencies above the BF, Z_{occ} appeared to make a transition to mass-dominated. However, in the Discussion section of that article, those conclusions were questioned, since, as noted above, the cochlear traveling wave should never reach the resonant point. So that aspect of the results, which was not robust (not seen in many cases), was not considered to be reliable. The inverse method of de Boer and Nuttall (34) used BM motion measurements and a 3D model to predict OCC impedance. They did not find a resonance, but again, such a resonance is not expected to be observed as the wave will stop before reaching it. Finally, Cooper and Rhode (45), measuring in a live apical guinea pig preparation, found no change in tuning after brushing off the OCC. This is pretty conclusive evidence that the OCC mass does not play a large role in tuning in the apex.

Influence of frequency-dependent stiffness

We noted at the outset that the idea that the stiffness is not frequency dependent is likely an oversimplification, particularly in light of the frequency dependence found by Scherer and Gummer (26). How would including a stiffness that increases with frequency (as their results show) influence our conclusions? In fact, a stiffness that increases with frequency would only emphasize the need for OCC mass for the cochlear wavenumber to vary with frequency as observed. This is because the effect of OCC mass is to make the effective stiffness decrease with frequency, and if the stiffness were increasing with frequency, even more mass would be necessary to provide the necessary decrease in effective stiffness with frequency.

More complex cochlear models

Some of the complexity that has been explored in 3D models bears on the unexpectedly apically decreasing mass apparent in our results. In particular, Taber and Steele (46) showed that the more limber osseous spiral lamina of the primate, compared to animals like the guinea pig, could account for the relatively large phase lags of the squirrel monkey at frequencies well below the best frequency. That sort of response is more like the relatively apical measurements we explored here, which did not have as flat a low frequency phase as the more basal results. Including this sort of detail in a cochlear model is likely required to sort out the physical properties that govern passive cochlear responses, and the role of local resonance in tuning.

Significance for the cochlear map

If local resonance is invoked as the basis of passive cochlear tuning, simple predictions can be made about the longitudinal stiffness variation needed to produce the observed cochlear map. The resonant frequency at any location depends on the square root of the local partition stiffness divided by the local mass, similar to a simple spring-mass resonant system. The OCC mass is usually assumed to be relatively invariant longitudinally. Then, for the gerbil, as the frequency map spans over two orders of magnitude, the (volumetric) stiffness needs to range over four orders of magnitude. Naidu and Mountain (42) measured the longitudinal variation of stiffness (at a point on the BM side) in gerbil. They found that the OCC stiffness did not decrease rapidly enough to supply a resonance-based explanation for the frequency map. Based on this discrepancy, they hypothesized the existence of a more complex motion, because a significant frequency-dependent variation in effective mass gradient is possible if the organ of Corti vibrates in a complicated fashion. However, Emadi et al. (43) also measured longitudinal point stiffness variations and drew the contrary conclusion—that the measured apical decrease in stiffness, with or without a slowly varying mass increase

(suggested by the anatomy), could supply the necessary stiffness gradient for a simple resonance-based cochlear map.

While our data started out supporting the idea of local resonance, the complete story has turned out to be more complicated. In the most basal measurements, the BF *is* just slightly less than the resonant frequency that is derived from our $k_{exp}(f)$ curves, supporting the idea of a resonance-based map. However, a little further apical, the apparent mass has decreased. This does not make sense in terms of a resonance-based map, since the stiffness will have to vary even more rapidly if mass is varying in the wrong direction. It has been pointed out by several authors (3,5,6) that the cochlear map can be produced without local resonance. Based on our results, local resonance is only likely to be important for setting the best frequency in the base, and has diminishing importance moving apically.

CONCLUSIONS

The basis for the cochlea's frequency tuning was explored by comparing theoretical predictions for the traveling wave wavenumber and direct measurements. This comparison was targeted at identifying the role that OCC mass plays in frequency tuning. This study was devised to apply in a frequency region below the resonance frequency, and not to look for the resonance directly. Based on the results of Cooper and Rhode (45), Scherer and Gummer (26), and the modeling results of Steele and colleagues (3,4,47), we rather expected to find that the OCC mass did not play a substantial role. However, the opposite was found. These results indicated that the OCC mass, by substantially decreasing the effective stiffness of the OCC, plays a leading role in passive cochlear tuning in the very base of the cochlea and a supporting role in slightly more apical positions within turn-one. Expanding our own measurements with the data and results of others reaffirmed this basic finding.

This study could be built upon: the main challenge to obtaining robust data was that k_{exp} could not be extended to frequencies very far above BF (where evanescent-fast wave dominated the response), so its extent in frequency was limited. Future experiments that could devise a way to extend the frequency range for measuring k_{exp} would be very useful. We used wavenumber to illuminate passive mechanics, but in addition, k_{exp} plays a critical role in feed-forward, feed-backward models that use longitudinally coupled outer hair cell forces to add energy to the cochlear traveling wave (8,47,48). Therefore, further and more advanced measures of k_{exp} could speak to active as well as passive mechanics.

We saw in Fig. 8 that the evanescent-fast modes may influence the calculation of OCC mass in the basal region and a caveat to these results is that the basal region of the cochlea is likely not well modeled by a rectangular box. Employing a 3D theory that is more true to the anatomy of this region would improve future efforts to match theoretical predictions to this well-explored cochlear region.

APPENDIX A: RELATION BETWEEN MODEL STIFFNESS AND POINT STIFFNESS MEASUREMENTS

The model stiffness we used in the equations above was defined as $S(x) = \Delta P(x)/\langle z\rangle$ (constant with frequency), where $\Delta P(x)$ is the pressure across the OCC at the longitudinal location x and $\langle z\rangle$ is the average displacement over one transverse section of the organ of Corti. It is the displaced area dividing by the length of the beam,

$$\langle z\rangle = \frac{1}{L}\int_0^{\mathrm{L}} z(y)dy.$$

S has units of dyne/cm^3. Point stiffness is found by measuring the force required to displace the BM at a point and has units of dyne/cm. The two can be linked via the beam equation that governs the bending of beams under both localized and uniform loads. The beam equation is

$$D\frac{d^4\mathrm{z}}{d\mathrm{y}^4} = q(y),$$

where $q(y)$ is the load, the force per unit length on the beam (dyne/cm). $D = EI$ is the flexural rigidity of the beam, a function of the beam height, width, and material, with units dyne cm^2. E is the Young's modulus and I is the moment of inertia. The y axis points along the length of the beam. The length of the beam, L, is the span of the BM. In beam theory, the load is uniform over the width of the beam. Below we solve the beam equation for a localized, centered load (point stiffness) and uniform pressure (model stiffness).

Uniform pressure load—model stiffness

We wish to find $S(x) = \Delta P(x)/\langle z\rangle$. The pressure is taken to be uniform on the beam, so $\Delta P(x) = \Delta P = P$. The beam equation becomes simply $D(d^4z/dy^4) = P\delta$ (with δ = beam width = probe diameter) and can be directly integrated as

$$z(y) = \frac{P\delta}{24D}y^4 + C_1y^3 + C_2y^2 + C_3y + C_4.$$

The constants are determined from the boundary conditions of the system. We present the solutions for two boundary conditions: for clamped edges (subscript c) and for the simply supported edges (subscript s).

The boundary conditions for clamped edges are $z = 0$ and $dz/dy = 0$ at $y = 0, L$, leading to

$$z(y) = \frac{P\delta}{24D}y^4 - \frac{P\delta L}{12D}y^3 + \frac{P\delta L^2}{24D}y^2 \quad \text{and} \quad \langle z\rangle_{\mathrm{C}} = P\delta L^4/720D.$$

The expression for the stiffness is $S_{\mathrm{C}} = P/\langle z\rangle_{\mathrm{C}} = 720D/\delta L^4$.

For the simply supported edges, the boundary conditions are $z = 0$ and

$$\frac{d^2z}{dy^2} = 0$$

at $y = 0, L$ leading to

$$z(y) = \frac{P\delta}{24D}y^4 - \frac{P\delta L}{12D}y^3 + \frac{P\delta L^3}{24D}y.$$

Then $\langle z\rangle_{\mathrm{S}} = P\delta L^4/120D$, resulting in $S_{\mathrm{S}} = P/\langle z\rangle_{\mathrm{S}} = 120D/\delta L^4$.

Localized load—point stiffness

The point stiffness case was treated by Gummer et al. (49). In this case the beam equation is

$$D\frac{d^4z}{dy^4} = \frac{F}{\delta}\{\mathrm{U}(\mathrm{y}-\mathrm{y}_0) - U(y-y_1)\}$$

(where U is the unit step function), and q is a constant $= F/(y_1\text{-}y_0) \sim F/\delta$. This can be solved by Laplace transform, following Gummer et al. Their analysis with a force applied to the center beam (their Eqs. 11 and 16) led to the following expression for point stiffness: in the clamped condition,

$$F/z|_{\mathrm{C}} = \frac{2880D}{15L^3}$$

and in the simply supported condition,

$$F/z|_{\mathrm{S}} = \frac{144D}{3L^3}.$$

By comparing point and model stiffness values to eliminate D, model stiffness, $S_{c/s}$ can be expressed as a function of point stiffness,

$$\left.\frac{F}{z}\right|_{\mathrm{C/S}},$$

BM width and probe diameter:

$$S_{\mathrm{C}} = \left.\frac{F}{z}\right|_{\mathrm{C}}(3.75/\delta L) \quad \text{and}$$

$$S_{\mathrm{S}} = \left.\frac{F}{z}\right|_{\mathrm{S}}(2.5/\delta L).$$

Experimental basilar membrane point stiffness measurements in gerbil

The BM width is taken equal to 165 μm (same value as for the model results above.) Table 1 assembles experimental point stiffness values and their corresponding model stiffness. Measurements were all recorded from the base of the gerbil cochlea. The value δ is the diameter of the probe. The model stiffness found in this article was 2–2.5 10^9 dyne/cm^3 at the more basal location (BF ~35–40 kHz) and 3–5 10^8 dyne/cm^3 at the slightly more apical location (BF ~20–25 kHz). These values overlap with those derived from the point stiffness measurements of Naidu and Mountain (42) and Olson and Mountain (41), and were in reasonable agreement—five or more times larger—with those predicted from the Emadi et al. (43) results.

TABLE 1

Ref. and comments	δ (μm)	Pt stiffness (dyne/cm)	S_c (dyne/cm^3)	S_s (dyne/cm^3)
(41), in vivo cochlea	20	~6500 = 6.5 N/m	7.4 10^8	4.9 10^8
(42), in vitro cochlea	10	~2200	5.0 10^8	3.3 10^8
(43), in vitro hemicochlea	25	~790	7.2 10^7	4.8 10^7

First column: Reference from which the data are quoted; comments about the experimental conditions. Second column: δ is the probe diameter in μm. Third column: Experimental point stiffness values. Fourth and fifth columns: Corresponding model stiffness for the clamped-edges condition (S_c) and for the simply supported condition (S_s). All the data were from the base of the gerbil cochlea; the width of the basilar membrane was taken equal to 165 μm (same value as for the model results).

APPENDIX B: EXPRESSION OF THE EFFECTIVE FLUID MASS AND THE DISPERSION RELATION FOR 1D AND 2D COCHLEAR MODELS

The following is only to sketch the equivalent height concept; more general treatments can be found in the literature (1,3,28). Imagine a vial of water (density ρ) of height h that is shaken (accelerated) up and down with acceleration $a_z(t)$. The vial is small enough that the fluid moves together; it does not slosh around. Then the pressure on the bottom of the fluid column is $p = a_z\rho h$ (plus a static term due to the fluid's weight, $p = g\rho h$). In the cochlea, when the OCC moves up and down, the pressure at the BM is responsible for accelerating the adjacent fluid layer in scala tympani. The height of this layer is not equal to the scala depth; due to the traveling wave, as one part of the BM is moving up another is moving down, the fluid moves in roughly a circular pattern, and not simply perpendicular to the BM in a column (1). Nevertheless, an equation relating the pressure at the BM and the acceleration at the BM can be written. To find it, generally one finds the solution to the Laplace equation, $\nabla^2 p = 0$ in the fluid, considering the boundary conditions and the dimensionality of the model, and also employs the Navier-Stokes equation for inviscid, linear flow, $\vec{\nabla}p = -\rho\vec{a}$. The result is an equation, $p = a_z\rho h_{\mathrm{eq}}$, where p is the pressure next to the BM and h_{eq}, the equivalent height of fluid, depends on cochlear dimensions and the local wavenumber of the cochlear traveling wave. To then find the dispersion relationship that relates wavenumber to frequency, the mechanics of the OCC is included. At the BM, the relation between the pressure p driving the OCC and its motion v_z is given by $v_z = -2p/Z_{\mathrm{occ}}$, with Z_{occ} the specific acoustic impedance of the OCC. Combining with the equation above for the fluid leads to $h_{\mathrm{eq}} = -Z_{\mathrm{occ}}/2_{i\omega\rho}$.

2D short-wave model of the cochlea

2D turns out to be simpler than 1D, so we start with it. Assuming that the BM motion is a wave, and taking the short-wave approximation, which assumes that the wavelength is much shorter than the scalae height, the pressure for the 2D model is given by $p(x,z) = p_0 e^{i(\omega t - kx)}e^{-kz}$. (It can easily be seen that this solves the Laplace equation, and the pressure goes to zero for large z, which is consistent with the short-wave approximation; note that with the short-wave approximation, the cochlear dimensions drop out.) From the Navier-Stokes equation, we have

$$\frac{dp}{dz} = -\rho a_z,$$

which leads to $kp = i\omega\rho v_z = p/h_{\mathrm{eq}}$. Therefore, the effective fluid mass for the 2D short-wave model is $h_{\mathrm{eq}} = Q_{\mathrm{2D-SW}} = 1/k$ (see in Fig. 2) and the dispersion relation is $k_{\mathrm{2D}} = -2i\omega\rho/Z_{\mathrm{occ}}$. For the simple case of a stiffness dominated OCC impedance, $Z_{\mathrm{occ}} = S/i\omega$, the dispersion relationship is simply $k_{\mathrm{2D}} = 2\omega^2\rho/S$; in a 2D model of the cochlea without OCC mass, the wavenumber goes as frequency squared.

1D model of the cochlea

The pressure for a 1D model is given by $p = p_0 e^{i(\omega t - kx)}$. In the 1D treatment, Laplace's equation is not used because the fluid motions and pressure variations are only allowed in the x direction. Conservation of fluid mass gives the relation

$$h\frac{dv_x}{dx} = \varepsilon v_z$$

(with h the height of the scala, and ε the width of the BM). This expresses that when the BM moves up (in the z direction), the x velocity of the fluid will increase in the x direction to make room. From the Navier-Stokes equation, we have

$$\frac{dp}{dx} = -\rho a_x = -i\omega\rho v_x.$$

After taking the derivative on both sides, we reach the equation

$$\frac{d^2p}{dx^2} = -i\omega\rho\,\frac{dv_x}{dx} \Leftrightarrow -k^2p = -i\omega\rho v_z\,\frac{\varepsilon}{h},$$

where we have used

$$\frac{d}{dx} = -ik, \quad \frac{d}{dt} = i\omega.$$

This leads to $h_{eq} = Q_{1D}(k) = \varepsilon/hk^2$ (see Fig. 2). Incorporating the relationship between p and the OCC impedance, we find

$$Q_{1D}(k) = -\frac{Z_{occ}(x)}{2i\omega\rho}$$

and therefore the dispersion relation for a 1D model is

$$k_{1D} = \sqrt{-\frac{2i\omega\rho\varepsilon}{hZ_{occ}}}.$$

When the OCC impedance is stiffness-dominated, $Z_{occ} = S/i\omega$ and $k_{1D} = \omega\sqrt{2\rho\varepsilon/hS}$; in a 1D model of the cochlea without OCC mass, the wavenumber goes as frequency. This is a nondispersive case, as the wave's velocity, $d\omega/dk$, does not vary with frequency.

We thank Shyam Khanna for guidance and assistance with the confocal interferometer. We are grateful to Nigel Cooper for sharing his gerbil basilar membrane motion data. We also thank Nigel Cooper, Wei Dong, and Egbert de Boer for commenting on previous versions of the manuscript, and the two anonymous reviewers for their help in improving the manuscript.

This work received support from the National Institute on Deafness and Other Communication Disorders and the Emil Capita Foundation.

REFERENCES

1. Lighthill, J. 1981. Energy flow in the cochlea. *J. Fluid Mech.* 106:149–213.
2. Edge, R. M., B. N. Evans, M. Pearce, C. P. Richter, X. Hu, and P. Dallos. 1998. Morphology of the unfixed cochlea. *Hear. Res.* 124: 1–16.
3. Steele, C. R., and L. A. Taber. 1979. Comparison of WKB calculations and experimental results for three-dimensional cochlear models. *J. Acoust. Soc. Am.* 65:1007–1018.
4. Steele, C. R., and L. A. Taber. 1981. Three-dimensional model calculations for guinea pig cochlea. *J. Acoust. Soc. Am.* 69:1107–1111.
5. Siebert, W. M. 1974. Ranke revisited—a simple short-wave cochlear model. *J. Acoust. Soc. Am.* 56:594–600.
6. Zwislocki, J. 1950. Theory of the acoustical action of the cochlea. *J. Acoust. Soc. Am.* 22:778–784.
7. Lim, K. M., and C. R. Steele. 2002. A three-dimensional nonlinear active cochlear model analyzed by the WKB-numeric method. *Hear. Res.* 170:190–205.
8. Wen, B. 2006. Modeling the Nonlinear Active Cochlea: Mathematics and Analog VLSI. University of Pennsylvania, State College, PA.
9. Lim, D. J. 1980. Cochlear anatomy related to cochlear micromechanics. A review. *J. Acoust. Soc. Am.* 67:1686–1695.
10. Kolston, P. J. 2000. The importance of phase data and model dimensionality to cochlear mechanics. *Hear. Res.* 145:25–36.
11. Ruggero, M. A., N. C. Rich, A. Recio, S. S. Narayan, and L. Robles. 1997. Basilar-membrane responses to tones at the base of the chinchilla cochlea. *J. Acoust. Soc. Am.* 101:2151–2163.
12. de Boer, E., and E. van Bienema. 1982. Solving cochlear mechanics problems with higher-order differential equations. *J. Acoust. Soc. Am.* 72:1427–1434.
13. Olson, E. S. 2001. Intracochlear pressure measurements related to cochlear tuning. *J. Acoust. Soc. Am.* 110:349–367.
14. Peterson, L. C., and B. P. Bogert. 1950. A dynamical theory of the cochlea. *J. Acoust. Soc. Am.* 22:369–381.
15. Cooper, N. P., and W. S. Rhode. 1996. Fast traveling waves, slow traveling waves and their interactions in experimental studies of apical cochlear mechanics. *Aud. Neurosci.* 2:289–299.
16. Johnstone, J. R., V. A. Alder, B. M. Johnstone, D. Robertson, and G. K. Yates. 1979. Cochlear action potential threshold and single unit thresholds. *J. Acoust. Soc. Am.* 65:254–257.
17. Sokolich, G. W. 1981. Closed sound delivery system. United States Patent 4251686.
18. Khanna, S. M., C. J. Koester, J. F. Willemin, R. Dandliker, and H. Rosskothen. 1996. A noninvasive optical system for the study of the function of inner ear in living animals. *SPIE.* 2732:64–81.
19. Willemin, J. F., R. Dandliker, and S. M. Khanna. 1988. Heterodyne interferometer for submicroscopic vibration measurements in the inner ear. *J. Acoust. Soc. Am.* 83:787–795.
20. Decraemer, W. F., O. de La Rochefoucauld, W. Dong, S. M. Khanna, J. J. J. Dirckx, and E. S. Olson. 2007. Scala vestibuli pressure and three-dimensional stapes velocity measured in direct succession in gerbil. *J. Acoust. Soc. Am.* 121:2774–2791.
21. de La Rochefoucauld, O., S. M. Khanna, and E. S. Olson. 2005. Recording depth and signal competition in heterodyne interferometry. *J. Acoust. Soc. Am.* 117:1267–1284.
22. de La Rochefoucauld, O., S. M. Khanna, and E. S. Olson. 2006. Signal competition in heterodyne interferometry. *In* 7th International Conference on Vibration Measurements by Laser Techniques: Advances and Applications. E. P. Tomasini, editor.
23. Olson, E. S. 2004. Harmonic distortion in intracochlear pressure and its analysis to explore the cochlear amplifier. *J. Acoust. Soc. Am.* 115: 1230–1241.
24. Watts, L. 2000. The mode-coupling Liouville-Green approximation for a two-dimensional cochlear model. *J. Acoust. Soc. Am.* 108:2266–2271.
25. Allaire, P., S. Raynor, and M. Billone. 1974. Cochlear partition stiffness—a composite beam model. *J. Acoust. Soc. Am.* 55:1252–1258.
26. Scherer, M. P., and A. W. Gummer. 2004. Impedance analysis of the organ of Corti with magnetically actuated probes. *Biophys. J.* 87: 1378–1391.
27. Olson, E. S. 1998. Observing middle and inner ear mechanics with novel intracochlear pressure sensors. *J. Acoust. Soc. Am.* 103:3445–3463.
28. de Boer, E. 1981. Short waves in three-dimensional cochlea models: solution for a ''block'' model. *Hear. Res.* 4:53–77.
29. de Boer, E. 1998. A method for forward and inverse solutions of a three-dimensional model of the cochlea. *J. Acoust. Soc. Am.* 103:3725–3729.
30. Plassmann, W., W. Peetz, and M. Schmidt. 1987. The cochlea in gerbilline rodents. *Brain Behav. Evol.* 30:82–101.
31. Muller, M. 1996. The cochlear place-frequency map of the adult and developing Mongolian gerbil. *Hear. Res.* 94:148–156.
32. Ren, T. 2002. Longitudinal pattern of basilar membrane vibration in the sensitive cochlea. *Proc. Natl. Acad. Sci. USA.* 99:17101–17106.
33. Rhode, W. S., and A. Recio. 2000. Study of mechanical motions in the basal region of the chinchilla cochlea. *J. Acoust. Soc. Am.* 107:3317–3332.
34. de Boer, E., and A. L. Nuttall. 2000. The mechanical waveform of the basilar membrane. III. Intensity effects. *J. Acoust. Soc. Am.* 107:1497–1507.

35. Cooper, N. P., and W. S. Rhode. 1992. Basilar membrane mechanics in the hook region of cat and guinea-pig cochleae: sharp tuning and nonlinearity in the absence of baseline position shifts. *Hear. Res.* 63: 163–190.

36. Rhode, W. S. 1971. Observations of the vibration of the basilar membrane in squirrel monkeys using the Mössbauer technique. *J. Acoust. Soc. Am.* 49:1218–1231.

37. Olson, E. S. 1999. Direct measurement of intra-cochlear pressure waves. *Nature*. 402:526–529.

38. Cooper, N. P. 2000. Basilar membrane vibrations in the basal turn of the gerbil cochlea. *In* 23rd ARO Midwinter Meeting (Association for Research in Otolaryngology), St. Petersburg Beach, FL.

39. Geisler, C. D., and Y. Cai. 1996. Relationships between frequency-tuning and spatial-tuning curves in the mammalian cochlea. *J. Acoust. Soc. Am.* 99:1550–1555.

40. Shera, C. A. 2001. Intensity-invariance of fine time structure in basilar-membrane click responses: implications for cochlear mechanics. *J. Acoust. Soc. Am.* 110:332–348.

41. Olson, E. S., and D. C. Mountain. 1994. Mapping the cochlear partition's stiffness to its cellular architecture. *J. Acoust. Soc. Am.* 95: 395–400.

42. Naidu, R. C., and D. C. Mountain. 1998. Measurements of the stiffness map challenge a basic tenet of cochlear theories. *Hear. Res.* 124:124–131.

43. Emadi, G., C. P. Richter, and P. Dallos. 2004. Stiffness of the gerbil basilar membrane: radial and longitudinal variations. *J. Neurophysiol.* 91:474–488.

44. Dong, W., and E. S. Olson. 2006. Middle ear forward and reverse transmission in gerbil. *J. Neurophysiol.* 95:2951–2961.

45. Cooper, N. P., and W. S. Rhode. 1995. Nonlinear mechanics at the apex of the guinea-pig cochlea. *Hear. Res.* 82:225–243.

46. Taber, L. A., and C. R. Steele. 1981. Cochlear model including three-dimensional fluid and four modes of partition flexibility. *J. Acoust. Soc. Am.* 70:426–436.

47. Steele, C. R., and K. M. Lim. 1999. Cochlear model with three-dimensional fluid, inner sulcus and feed-forward mechanism. *Audiol. Neurootol.* 4:197–203.

48. Geisler, C. D., and C. Sang. 1995. A cochlear model using feed-forward outer-hair-cell forces. *Hear. Res.* 86:132–146.

49. Gummer, A. W., B. M. Johnstone, and N. J. Armstrong. 1981. Direct measurement of basilar membrane stiffness in the guinea pig. *J. Acoust. Soc. Am.* 70:1298–1309.